A clear-sky radiance archive from Meteosat "water vapor" observations

Hélène Brogniez,[1,2] Rémy Roca,[3] and Laurence Picon[3]

Received 28 February 2006; revised 14 June 2006; accepted 24 July 2006; published 8 November 2006.

[1] A long-term archive of clear-sky Meteosat "water vapor" observations, covering the July 1983 to February 1997 period with a 3 hourly time step and a spatial resolution of 0.625°, is presented. Cloud clearing is performed using a scene selection procedure based on the International Satellite Cloud Climatology Project DX product. In this procedure low cloud scenes are kept because of the negligible contribution of the low atmospheric layer in this spectral band. Cloud contamination is shown to have little influence on the clear-sky radiance (CSR) field and is mainly confined to the continental Intertropical Convergence Zone with values less than 0.5 K. This scene selection yields to a significantly enhanced sampling with respect to pure clear-sky in the subtropical high regions. Homogenization of the 14 year database is performed in accordance with existing technique. A comparison to the operational radiosondes archive indicates a small bias of 0.3 K that is stable throughout the period. A first analysis of the CSR variability reveals that the intraseasonal variance over the subtropical dry regions has a strong seasonal cycle in the Northern Hemisphere that is not observed in the Southern Hemisphere. Such a data set completes the ones currently available to document the water vapor variability of the troposphere from climatic down to regional and daily scales.

Citation: Brogniez, H., R. Roca, and L. Picon (2006), A clear-sky radiance archive from Meteosat ''water vapor'' observations, *J. Geophys. Res.*, *111*, D21109, doi:10.1029/2006JD007238.

1. Introduction

[2] Water vapor is an important element of the atmosphere composition and is usually thought to play a central role in the climate system through a strongly positive radiative feedback loop [e.g., *Held and Soden*, 2000; *Bony et al.*, 2006]. Computation of the impact of humidity perturbations on the outgoing longwave radiation at the top of the atmosphere reveals that (1) the free troposphere is the most sensitive region of the atmosphere to such perturbations and (2) this sensitivity increases with the dryness of the atmosphere [*Spencer and Braswell*, 1997]. This nonlinearity points toward the intertropical free troposphere as a key element of the longwave radiative budget of the Earth [*Pierrehumbert*, 1995]. Unlike in the turbulent boundary layer where the local temperature structures drive the humidity content, the relative humidity distribution in the free troposphere is governed by large-scale dynamics and long-range transport [e.g., *Pierrehumbert and Roca*, 1998; *Waugh*, 2005]. As a result, the dynamics of water vapor in the free troposphere span a large range of scale from the basin wide subtropical dry subsiding zones down to the synoptic-scale filamentary structures evident on satellite imagery [e.g., *Morel et al.*, 1978], idealized models simulations [e.g., *Joseph and Moustaoui*, 2000] and General Circulation Models (GCM) simulations outputs [*Yang and Pierrehumbert*, 1994] or in situ measurements [*Marenco et al.*, 1998].

[3] The observational characterization of such a multiscale variable is an ambitious challenge for which the operational meteorological satellites archive appears well suited. Indeed, infrared radiometers on board the geostationary orbit readily offer half-hourly depiction of the emitted radiation around the 6.3 μm water vapor absorption band. In this band, the measured signal is related to the humidity content of the free troposphere [e.g., *Ramond et al.*, 1981] that can be easily transformed, in the tropics, into a mean relative humidity of a broad layer [*Schmetz and Turpeinen*, 1988; *Soden and Bretherton*, 1993]. Furthermore, such data have been acquired continuously for a long time. For instance the series of Meteosat satellites started in 1977 with a high spatial resolution of a few kilometers and half hourly time step. A degraded version of this data set is available through the International Satellite Cloud Climatology Project (ISCCP) and covers continuously the period from July 1983 onward at a 3 hourly time step and an equivalent resolution of 30 km. We use here this data set which provides a long time series of raw ''water vapor'' (WV) radiances well suited to characterize the water vapor variability in the free troposphere at different scales.

[1]Department of the Geophysical Sciences, University of Chicago, Chicago, Illinois, USA.
[2]Now at Centre d'Etude des Environnements Terrestre et Planétaires, Centre National de la Recherche Scientifique, Institut Pierre-Simon Laplace, Velizy, France.
[3]Laboratoire de Météorologie Dynamique, Centre National de la Recherche Scientifique/Institut Pierre-Simon Laplace, Paris, France.

0148-0227/06/2006JD007238

[4] A number of processing steps are nevertheless necessary prior to the quantitative use of such a data set. First the long-term archive needs to be homogeneous over its time span. Indeed, the succession of slightly evolving radiometers over the years, from Meteosat-1 to Meteosat-5, as well as the modernization/evolution of the vicarious calibration techniques yield to strong artificial changes in the raw times series. Such inhomogeneities can be accounted for and corrected following the technique introduced in our reference paper [*Picon et al.*, 2003, hereinafter referred to as P03]. Such homogenous total sky radiance database can be use as is for a number of applications like model evaluations; be it climate [*Roca et al.*, 1997; *Ringer et al.*, 2003] or cloud resolving models [*Diongue et al.*, 2002] as well as for direct climate analysis of the total sky radiance variability [e.g., *Picon and Desbois*, 1990]. But other important applications require clear-sky radiances: assimilation in variational schemes for atmospheric reanalysis production [*Köpken et al.*, 2003], humidity retrieval [e.g., *Soden and Bretherton*, 1993; *Bates and Jackson*, 2001; *Brogniez et al.*, 2004], climate analysis of the brightness temperature [*Wu et al.*, 1993] or general circulation model evaluation [e.g., *Soden and Bretherton*, 1994; *Allan et al.*, 2003; *Brogniez et al.*, 2005].

[5] The clear-sky radiances (CSR) are obtained after a cloud clearing or clear-sky scene selection applied on the data. It is usually based on ancillary window infrared channels results [e.g., *Soden and Bretherton*, 1993] or a combination of ancillary data and radiative transfer computations [e.g., *Udelhofen and Hartmann*, 1995]. The CSR are sometimes produced in the satellite data operators, like NOAA, where it inherited the clear-sky selection procedure used for sounding [*McMillin and Dean*, 1982], or EUMETSAT, where the clear-sky selection is based on a clustering approach (provided by the Climate Data Set). An important characteristic of the 6.3 μm channel of Meteosat concerns its general insensitivity to the lowest level of the atmosphere. As shown in the pioneer work of *Schmetz and Turpeinen* [1988], the use of this channel should hence not be limited to pure clear-sky scenes but extended to the scenes where low-level cloudiness is present but does not influence the "water vapor" radiance. This calls for a more elaborated clear-sky scene selection that includes cloud vertical information rather than a simple cloud masking approach.

[6] In the intertropical belt, such an enhanced sampling is important owing to the frequently observed oceanic low-level stratus and stratocumulus large decks. The resulting gain of sampling serves two objectives: first at the individual time step, it increases the spatial cover for which the CSR become available which makes possible the building of useful daily mean maps. Second at the monthly timescale and for areas of high spatial and temporal variability, it increases the reliability of the mean value and provides significant monthly standard deviation based on these daily values. In the Intertropical Convergence Zone (ITCZ), it is expected to reduce the so-called "dry bias" that is known to affect IR-derived Upper Tropospheric Humidity (UTH) climatology when compared to radiosondes climatology for instance [*Soden and Lanzante*, 1996; *Lanzante and Gahrs*, 2000] by sampling the near environment of deep convection. Bad cloud tops attribution and/or detection could nevertheless result in a cloud contamination of the CSR. This can bias the comparison with operational advanced assimilation systems [*Köpken et al.*, 2003] or the evaluation of a geophysical parameter like UTH, also sometimes referred to as FTH (Free Tropospheric Humidity) because of the widening of the observed atmospheric layer over the subsiding areas [*Brogniez et al.*, 2005], from the CSR. As a result, such a selection of clear-sky scenes can be critical and one needs to find the fair trade between enhanced sampling and minimal cloud contamination of the radiances.

[7] In this paper, we extend our previous work on the Meteosat archive and now propose a new homogenous long-term archive of the clear-sky radiance of the water vapor channel. First, the data used to perform the cloud clearing as well as the rationale for the clear-sky scene selection are presented in details. The methodological issues are also highlighted. Section 3 is dedicated to the analysis of the sensitivity of the approach to the cloud detection scheme used. Examples of the sampling gains and limitations due to cloud clearing as well as some effect of the cloud contamination on the clear-sky brightness temperature (BT) are provided. In section 4, we evaluate the database against the radiosondes archive and establish its stability over the 1983–1996 period. Some considerations on absolute calibration are also given. A summary and conclusions are finally provided together with a first presentation of the water vapor variability over tropical Atlantic and Africa as revealed by the database.

2. Data and Methodology

2.1. International Satellite Cloud Climatology Project (ISCCP) Data

[8] The DX product from the ISCCP project [*Rossow and Schiffer*, 1991] consists in a number of cloud characteristics as well as the observed raw radiances provided at the DX pixel resolution. This corresponds to an under sampling of one pixel out of 6 in each directions of the original measurements and a temporal resolution of 3 hours in the case of geostationary platform. In our case, only the results from the processing of the Meteosat observations are used. Both observed raw radiances in the WV band and the cloud information are available from 1983 to 1997. (The ISCCP archive has recently been extended up to December 2004.) The cloud detection and parameters retrieval is fully described by *Rossow and Schiffer* [1991], *Rossow et al.* [1991] and *Rossow and Schiffer* [1999]. The technique relies on the use of infrared radiances (IR) together with visible (VIS) reflectances when available and consists in two steps: the cloud detection and the cloud level attribution.

[9] The first step is based on the analysis of the spatial variance [e.g., *Coakley and Bretherton*, 1982] of the IR radiances and VIS reflectances as well as on temporal variations with respect to previously established background climatology. The cloud mask is hence available at pixel scale every 3 hours over the Meteosat region. The second step requires ancillary data (temperature and humidity profiles) derived from the TOVS instrument on board the NOAA polar orbiting satellites, at a daily rate, to characterize the vertical structure of the atmospheric column. The cloud top pressure (P_{top}) is first determined with the IR

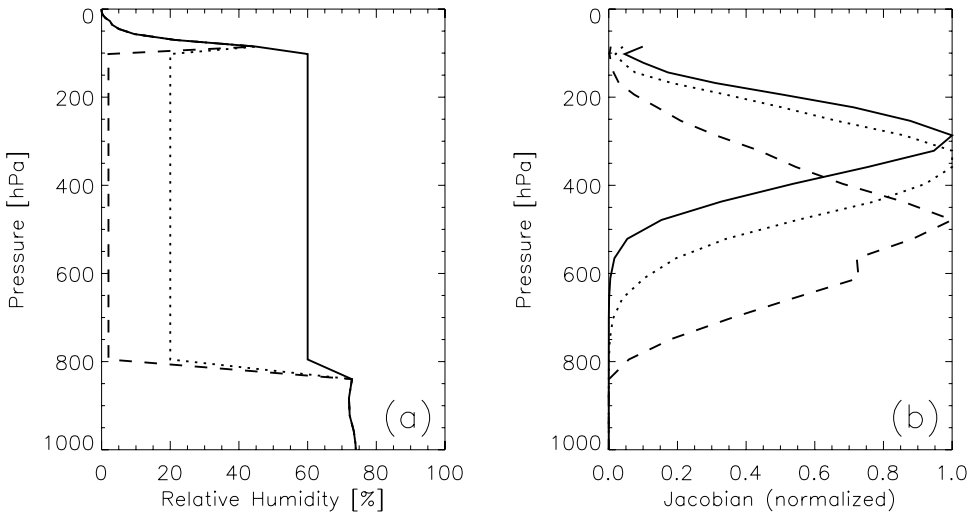

Figure 1. (a) Idealized relative humidity profiles with constant values in the 800–100 mbar layer: 60% (solid line), 20% (dotted line) and 2% (dashed line). In the boundary layer and in the stratosphere the relative humidity is from a standard tropical atmosphere [*McClatchey et al.*, 1971]. (b) Associated relative humidity Jacobian function of the Meteosat WV brightness temperature (∂BT/∂RH).

radiance only, assuming the cloud is opaque. Then depending upon availability, the VIS reflectance-derived albedo is converted into optical depth which allows for a so-called semitransparency correction of the P_{top} level attribution.

[10] The cloud detection algorithm has been designed to be cloud-conservative: it minimizes the risk of a false detection of cloud but may flag as clear, some cloudy scenes that resemble to clear-sky conditions. This detection technique makes use of both channels but the difference between day and night conditions mainly occurs because of this misdetection being more frequent at night when the VIS reflectance is not available [*Rossow and Garder*, 1993]. The cloud types affected by this misdetection are the subpixel fair weather cumulus as well as fog conditions. As discussed in the previous section, such misclassification only concerns low-level cloudiness that is, in our final aim, associated to clear-sky scenes. Hence the potential lowest reliability of the cloud mask construction using IR only data with respect to the bispectral approach is not a limiting factor in our clear and low cloud scene selection.

[11] On the other hand, the second step of the DX processing could influence our clear-sky radiance products more seriously. Indeed, if an actually mid-to-high cloud is erroneously associated to a level lower than 680 hPa, hence kept in our scene selection, this will contaminate the CSR. More generally errors in the evaluation of the cloud top pressure for low-level cloudiness could bias the selection of scenes. In the case of maritime boundary layer cloudiness over subtropical highs, the cloud top temperatures derived from ISCCP-DX VIS/IR algorithm have nevertheless been compared within 1–2 K to both in situ estimates [e.g., *Minnis et al.*, 1992] and to AVHRR alternative retrievals [*Mathieu et al.*, 2003]. For a typical dry lapse rate (10 K/km), such a small uncertainty results in less than 50 hPa uncertainty on the cloud top pressure. On the other hand, thin cirrus are less well characterized even though the cirrus detection has improved in the D series from the previous C products [*Stubenrauch et al.*, 1999], especially when multilayered situations are found (cirrus above low-level stratus decks) for which the algorithm tends not to detect the cirrus and associates the scene with low-level cloudiness [*Jin and Rossow*, 1997].

2.2. Rationale for Scene Selection

[12] The rationale for the scene selection is articulated around two points: the Meteosat "water vapor" channel spectral characteristics and the climatologic features of cloudiness in the Tropics and Subtropics. The Meteosat WV channel is sensitive, in clear sky, to the water vapor distribution in the troposphere and behaves similarly to the window channel in the presence of cloud. The actual layer that influences the signal nevertheless depends upon the geometry of view and the thermodynamical profile under consideration as shown in Figure 1. The Jacobians functions are calculated for a set of idealized tropical and subtropical profiles using the RTTOV-7 radiative transfer model [*Matricardi et al.*, 2004]. These computations confirm that, all other things being equal, the sensitive layer is broader and peaks lower in the atmosphere in a dry environment that in a moister environment [*Fischer et al.*, 1981]. It also shows that even in these extreme cases, the moist boundary layer (up to 800 hPa) hardly contributes to the observed radiance. From these characteristics, it has been proposed that retrieval and use of the data can be achieved in situations where low clouds are present in the column given that their tops are low enough not to contaminate the atmospheric signal [*Schmetz and Turpeinen*, 1988]. Figure 2 presents some estimates of such effects in a set of idealized computations. In the case of a moist profile, the actual sensitive layer peaks high enough in the troposphere (Figure 1) so that even a cloud topping up to 550 hPa does not influence the signal. On the other hand, in the very dry case, clouds cool the radiance as soon as they reach 800 hPa or so. In the intermediate case, contamination occurs for tops reach-

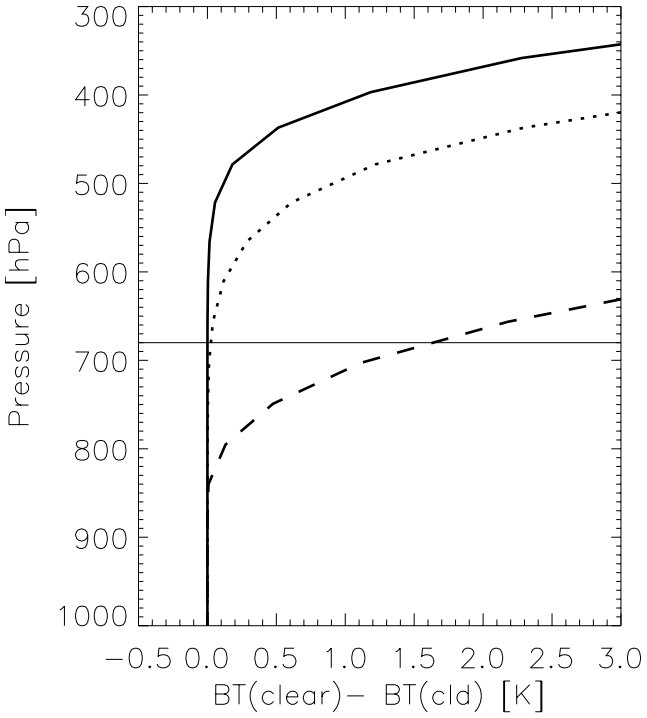

Figure 2. Difference (in Kelvins) between the clear-sky BT and the BT computed for a black cloud located at each pressure level as a function of pressure in the three idealized profiles of Figure 1 (solid line, RH = 60%; dotted line, RH = 20%; dashed line, RH = 2%). The horizontal line indicates the 680 hPa threshold.

ing 700 hPa. This value was previously used as a threshold [*Schmetz and Turpeinen*, 1988; *Udelhofen and Hartmann*, 1995] and implies, in our academic tests, a maximum contamination of 1.75 K in the very dry case (worst case scenario) and basically no effect for moister profiles.

[13] The second point of importance to the rationale concerns the climatology of cloudiness over the tropical part of the Meteosat field of view. Over the subtropical oceans low-level cloudiness is generally associated with trade winds cumuli which are located at the top of the maritime boundary layer around 850 hPa and spans large part of the subtropical Atlantic Ocean [e.g., *Picon et al.*, 1995]. These characteristics are presented at length in the following section but briefly, the average cloud top pressure for low-level cloudiness from the ISCCP-DX data over July 1992 is 820 hPa with a standard deviation of 40 hPa. Figure 2 indicates that such cloud at 800 hPa hardly contaminates the brightness temperature, but for a modest 0.5 K cooling in the very dry case indicating that the Meteosat WV channel is exploitable as if it was clear sky over most of these low-level cloudiness scenes. Hence following EUMETSAT early effort, we will refer in the following to the term clear-sky radiances (CSR) for brightness temperatures obtained by selecting scenes with either pure clear sky or populated with low-level clouds topping below a certain pressure threshold.

[14] For consistency with the ISCCP cloud products, a threshold of 680 hPa (instead of 700 hPa for EUMETSAT) is selected. To insure continuity and stable quality of the cloud level attribution procedure (the sensitive part of the scene selection process), over day and night, the clear and low cloud scene selection should rely on the cloud properties derived from the IR-only radiances analysis. Cloud contamination of the clear-sky radiance mainly occurs when a mid to upper tropospheric cloud is attributed erroneously to a P_{top} below 680 hPa, which is typically the case for the tops of the semitransparent thin cirrus which, in the IR-only framework, are not corrected for their departure from blackbodyness.

3. Evaluation of the Clear-Sky Radiance Products

[15] In the following, we evaluate the gains and the limitations of the degraded IR-only approach of selecting scenes as well as the sensitivity of the technique to the pressure threshold. The outputs from the VIS/IR algorithm are considered as the reference in the comparison and hence results are computed for 1200 UT only to insure good illumination conditions for the VIS channel. The CSR product consists in the averaging of the clear-sky and qualified low-level cloudiness DX pixels over a regular longitude latitude grid at the resolution of 0.625° × 0.625°. The nearest-neighbor regridding algorithm yields to fill each grid mesh with 1 to 9 DX pixels, depending upon departure from nadir, but only clear/low clouds pixels (with cloud top pressure below 680 hPa) are kept in the averaging. For clarity, the discussion below first focuses on the errors at the ISCCP pixel level and then the contamination of the gridded CSR products is evaluated.

3.1. Cloud Contamination Due to the Use of the IR-Only Algorithm

[16] The spatial distribution of the differences between the IR-only technique and the reference is revealed in Figure 3. The monospectral approach indeed yields to a general overestimation of the low cloud cover (41%) with respect to the VIS-IR algorithm (33%). The midlevel clouds are similarly detected by both techniques (14% versus 15%) while high clouds are more frequent in the VIS-IR approach (16%) than in the IR-only case (13%). The low-level cloudiness and high-level cloudiness differences seem mainly to occur over the continent. Over the ocean, the major difference appears to be restricted to the midlatitudes of the Southern Hemisphere. The level attribution errors are quantified and detailed in Figure 4 which summarizes the cloudiness characteristics obtained from the two algorithms for July 1992 at noon over a large region covering 45°N–45°S/45°W–45°E. It shows the statistics of the projection of the IR-only algorithm results in the VIS-IR technique: for each pixel, the IR-only results are listed within each of the available classes and the readings of the VIS-IR technique are incremented in these vertical categories accounting for the optical depth based subcategory. Almost all the IR-only detected high clouds are indeed high clouds in the VIS-IR approach. 1% should have been classified into midlevel cloudiness to fully reproduce the reference. Similarly, the majority of the IR-only midlevel cloudiness appears well associated to this level category in the reference, except for nearly 20% of the case that should have been classified in the high clouds category. These two misattributions of the

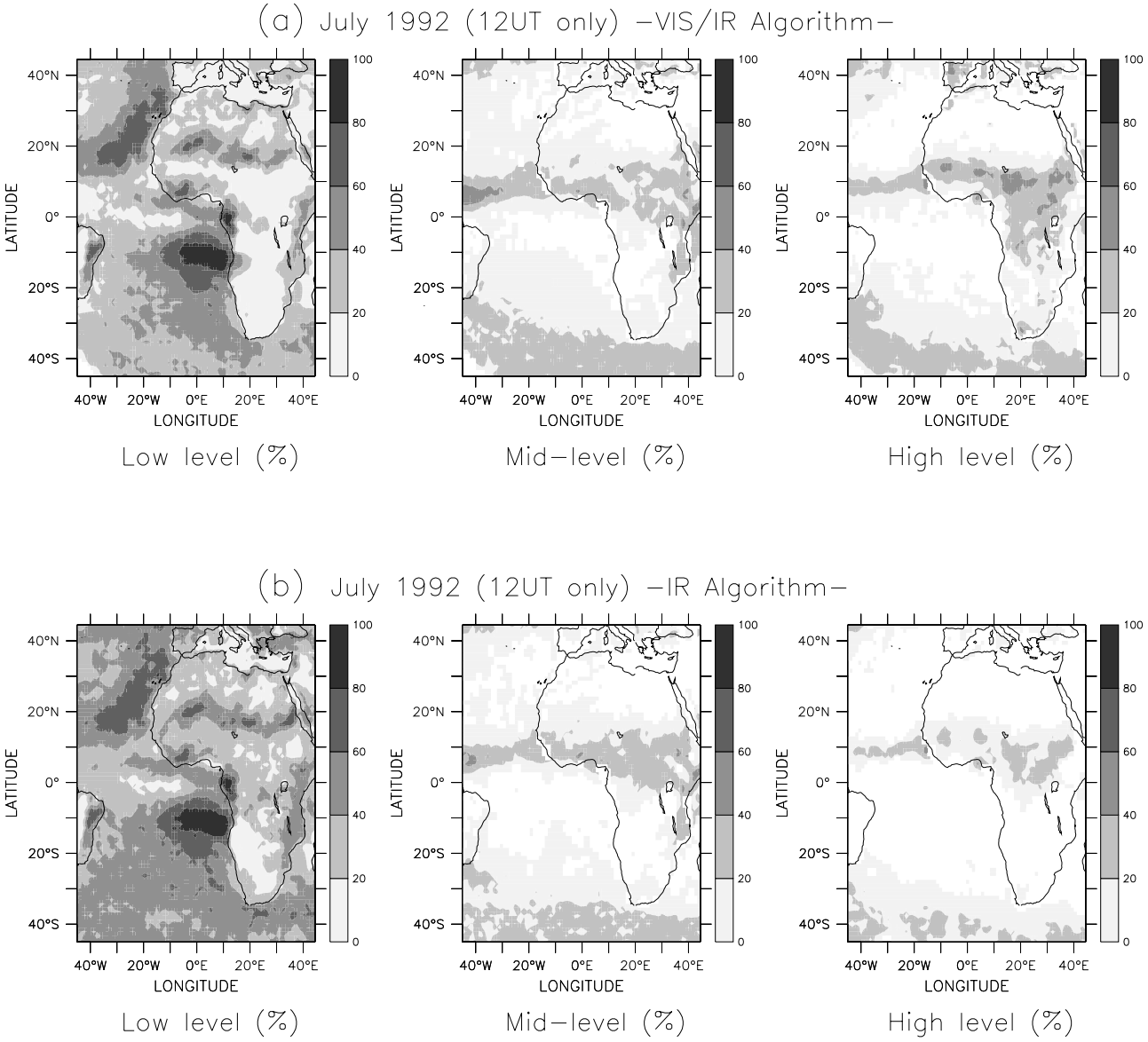

Figure 3. Maps of percentage of low-level ($P_{top} \geq 680$ hPa), midlevel (440 hPa $\leq P_{top} < 680$ hPa) and high-level ($P_{top} < 440$ hPa) cloudiness for July 1992 derived from (a) the VIS-IR algorithm and (b) the IR-only algorithm. Only the 1200 UT observations are used.

cloudiness levels are nevertheless not relevant to the scene selection which rejects both these subtype of clouds and do not result in cloud contamination of the CSR. In the more important case of the low-level cloudiness, Figure 4a indicates that 81% (33%+47%+1%) of the pixels detected by the IR-only algorithm are correctly classified, while the other 19% should be redistributed in equal parts into the high-level (10%) and midlevel (8%+1%) categories. The previously noted differences of behavior over land and sea are confirmed in Figures 4b and 4c. Indeed, over land (Figure 4b), 29% of the IR-only low clouds should have been put in the mid (9%+1%) and upper (19%) level category. Over sea (Figure 4c), only 13% of the low-level cloud pixels are misattributed (8%+1% in the mid level category and 4% in the high-level category). As expected, most of these misattributed pixels are associated to the lower optical depth category ($\tau < 3.6$). The high-level (midlevel) misclassified cases indeed have optical depth of 0.3 ± 0.2 (1.2 ± 0.8) and P_{top} of 160 ± 103 hPa (590 ± 68 hPa, respectively). Idealized computations of the impact of such a typical semitransparent high-level cirrus case (100% cloud cover at 200 hPa, optical depth of 0.3 or emissivity of 0.45 assuming a radius of 30 μm for equivalent spherical ice particles and the absorption coefficient of *Smith and Shi* [1992]) on the clear-sky brightness temperature are presented in Figure 5. The BT contamination reaches 7 K, 9 K and 13 K for the moist, intermediate and dry profiles, respectively. In the midlevel cloud case, (100% cloud cover at 600 hPa, optical depth of 1.2 or emissivity of 0.65 assuming a radius of 10 μm for equivalent spherical water droplets), the idealized computations indicate contamination smaller than 0.1 K

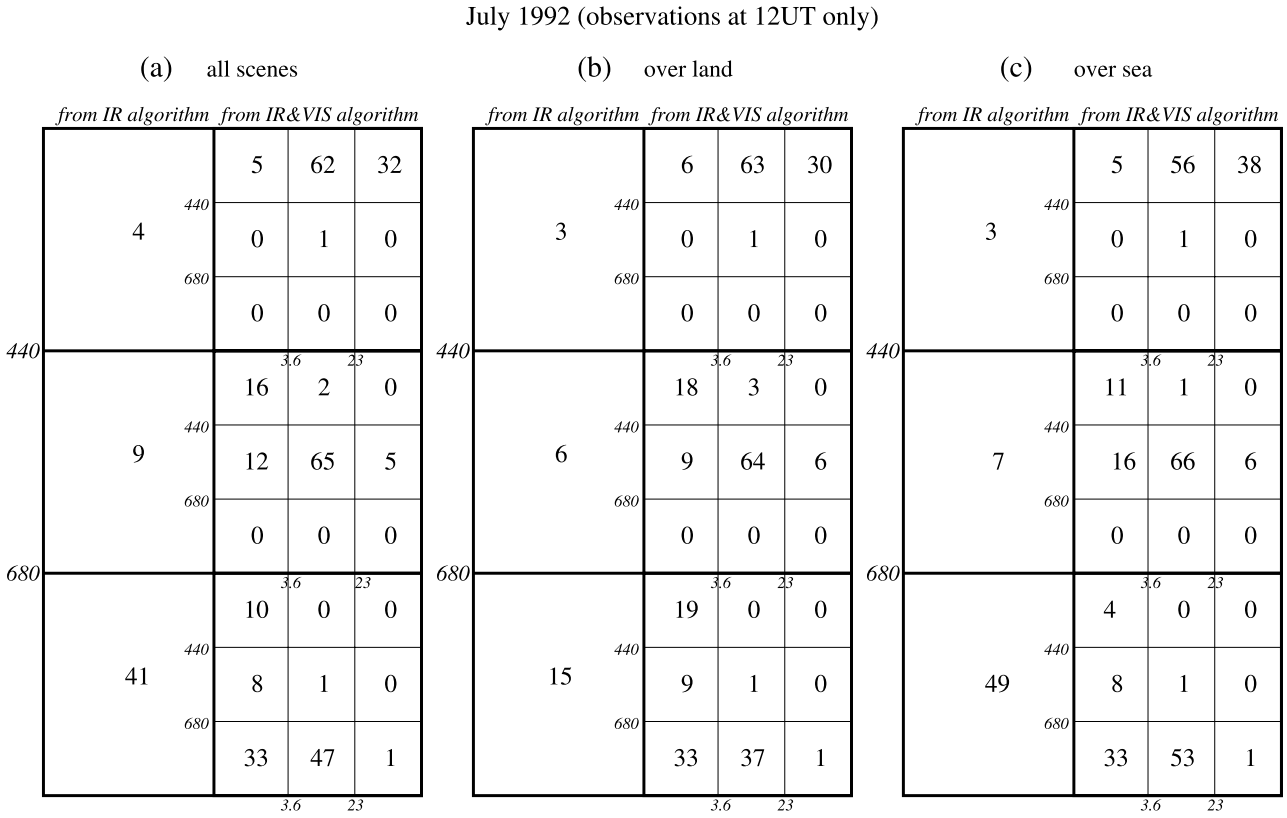

Figure 4. Distribution (in percent) of the ISCCP-DX pixels according to their cloud top pressure (P_{top} in hPa, vertical axis) from the IR radiance analysis, and their redistribution into the 9 ISCCP cloud types with the VIS reflectance (optical thickness on the horizontal axis). The distributions are performed for the 1200 UT images for the month of July 1992, and the percentages take into account the clear-sky pixels. (a) Global distribution over the area 45°W–45°E/45°N–45°S, (b) distribution over land, and (c) distribution over sea.

for the moist and dry conditions and of the order of 2.3 K for the very dry profiles (Figure 3b). Note that these estimates of bias are larger (smaller) if the misclassified cloud is thicker or higher (thinner or lower).

[17] The final CSR contamination is nevertheless very less than these theoretical, pixel-level instantaneous estimates because the pixel misclassification occurs over only part of the CSR mesh most of the time. Figure 6a shows this

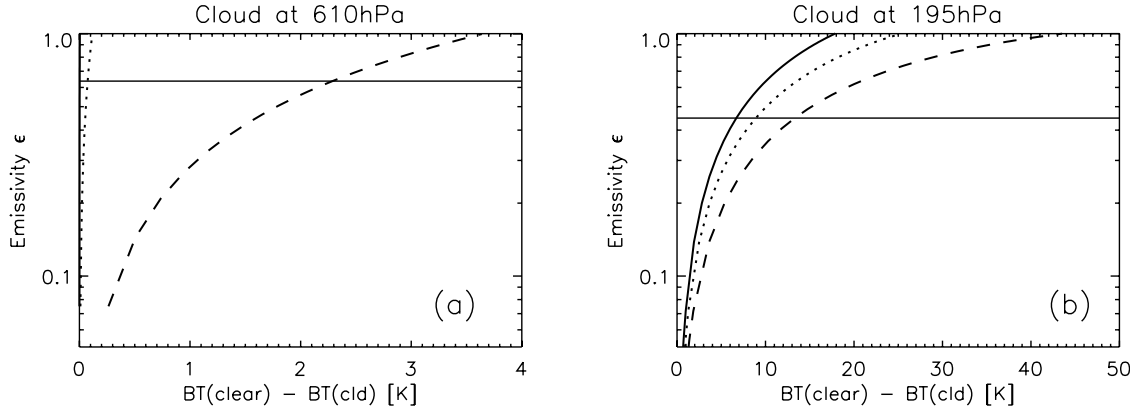

Figure 5. Influence of a cloud on the "water vapor" brightness temperature (BT in Kelvins), BT(cld), with respect to the clear-sky value, BT(clear), as a function of its emissivity. The cloud is located at (a) 600 hPa and (b) 200 hPa in the three idealized profiles of Figure 1 (solid line, RH = 60%; dotted line, RH = 20%; dashed line, RH = 2%). The horizontal lines show the cloud of optical thickness of 1.2 (emissivity = 0.65) and 0.3 (emissivity = 0.45) at 600 hPa and 200 hPa, respectively.

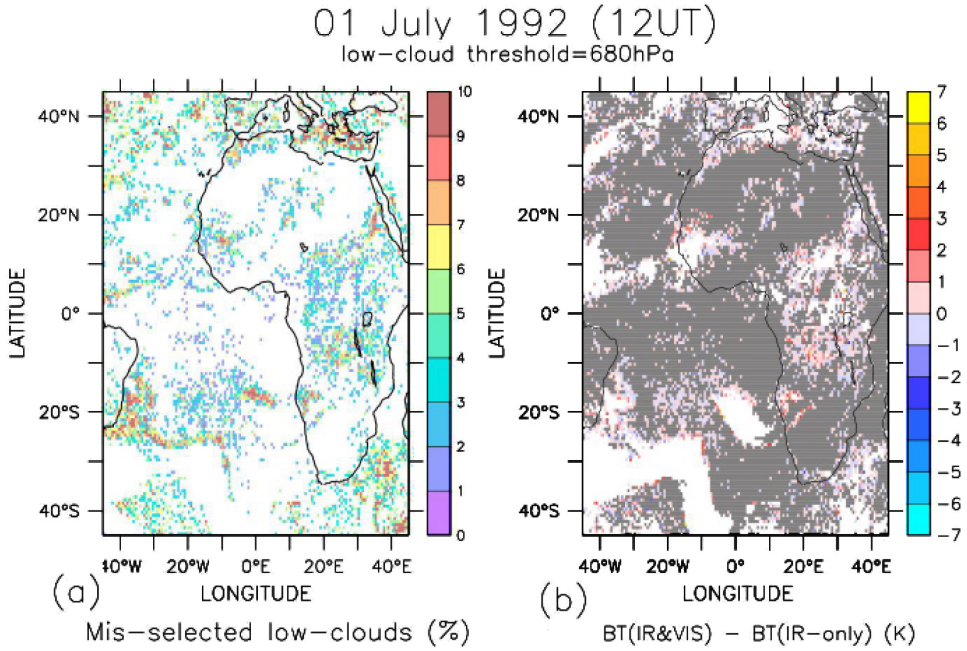

Figure 6. (a) Percentage of mis-selected low clouds within a so-called clear-sky radiance (CSR) mesh for the 1200 UT observation of 1 July 1992. (b) Difference in Kelvins for the same time step between the CSR derived from the VIS-IR algorithm and the CSR derived from the IR-only algorithm. The gray shading indicates differences equal to 0 K, and the white areas are scenes of missing values (no clear-sky or low-level cloud). For both figures the low clouds are selected using a threshold on the P_{top} of 680 hPa.

percentage of misclassification within a CSR mesh for 1 July 1992 at 1200 UT. It indicates that the different degrees of misclassification are present over both land and sea, in the subtropical highs regions as well as within the ITCZ. While the magnitude of the theoretical values should hold for the mesh with high fraction of misclassification, in the case of meshes with less than 100% errors with both algorithms (for which the computation of the CSR difference is possible), the BT difference is smaller (Figure 6b). On average over the region, the instantaneous difference vanishes to 0.04 K ± 0.32 K. The extrema of the difference reaches −4 K to +6.4 K depending upon the percentage of misclassification and the height/emissivity combined characteristics of the missed clouds. While the positive difference arises as expected from mis-selected mid-to-upper levels thin cirrus clouds by the IR only technique, the negative difference is associated to situations where the low-level cloud pixel that is kept in the IR-only technique is not a low-level cloud according to the VIS-IR algorithm. While this pixel is not considered to build the reference CSR based on the VIS-IR technique, it is associated to a free troposphere dryer than the surrounding environment, yielding to a IR-only CSR warmer than the reference. Such situation could occur in the case of partly cloudy scenes, involving for instance fair weather cumulus (see section 2.1).

[18] At the monthly timescale, the departure in Kelvin from a CSR built using the results from the IR-only algorithm or the VIS-IR technique smoothes out to 0.05 K (0.03 K) on average in January (July 1992) with standard deviation of 0.05 K (0.04 K) and maximum absolute value of the departure of 0.3 K (0.4 K) respectively, which is reached for a small group of meshes. The spatial distribution of this difference (Figure 7) shows that most of these errors are associated with the continental ITCZ over which patchy local maxima (0.2 K) are seen. Elsewhere the map reveals no particular patterns and differences are almost zero. It indicates that these small errors are associated to a randomly distributed misclassification of clouds. Hence the CSR built using the IR-only approach does not suffer from any systematic cloud contamination, besides a small bias over part of the continental ITCZ that could have been corrected for by using the VIS-IR approach.

3.2. Evaluation of the Gain in Sampling

[19] Because of the above detailed scene selection, more DX pixels qualify for the CSR meshes than if a simple cloud/no cloud mask were used. Note that the CSR product derived from the IR-only approach is considered in the following. Figures 8a and 8b show the spatial distribution of the resulting difference in CSR availability for an individual time step by considering pure clear-sky scene selection and the result of the above detailed selection. The gain in sampling in the warm (and dry) region in the southern tropical Atlantic is drastic. More generally, in the pure clear-sky case, a CSR value can be estimated for 58% of the mesh over the region while the elaborated scene selection yields CSR over up to 88% of the grid meshes. When daily means are constructed, either by using two samples to mimic polar orbiter sampling conditions (Figures 8c and 8d) or by using the eight available Meteosat images (Figures 8e and 8f), the sampling gain is confirmed although it is visually less impressive than for the individual slot. The mean built using eight images per day and the clear and low clouds scenes provides an estimate of daily mean CSR over 98% of the region versus 76% in the polar orbiter simulations using pure clear-sky selection. The significance of the former

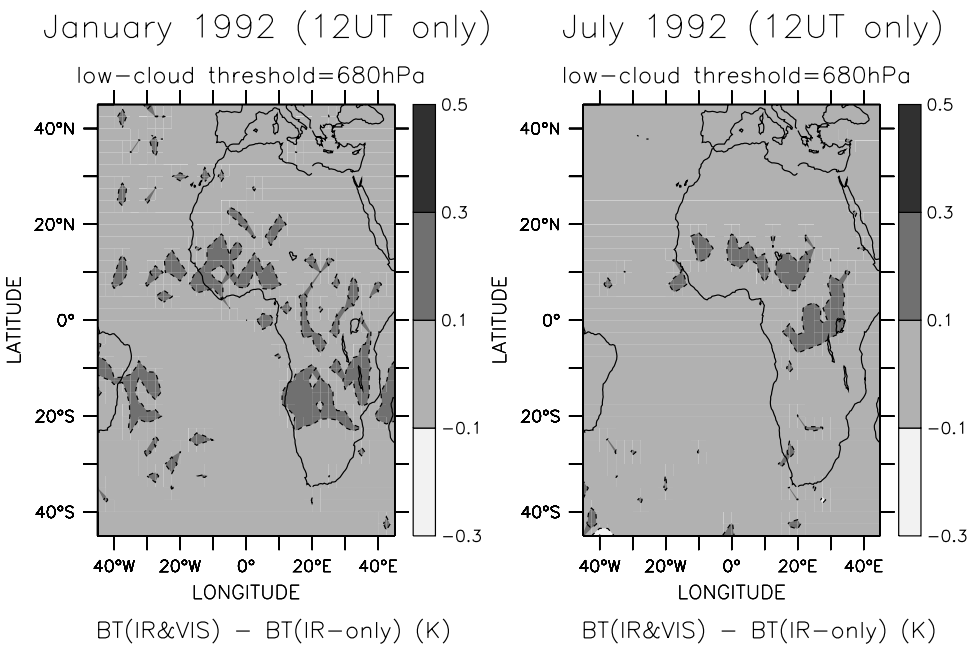

Figure 7. Difference in Kelvins between the monthly means CSR derived from the VIS-IR algorithm and the IR-only algorithm. For both algorithms the low-level clouds are below 680 hPa. The difference is determined for the 1200 UT observations of January 1992 and July 1992.

daily mean is estimated by computing the number of instantaneous CSR available per day. It averages to 7.1 (standard deviation s = 1.8) versus only 5.7 (s = 2.4) for pure clear-sky conditions. The spatial distribution (not shown) reveals that the gain is spread evenly across the ITCZ region and the subtropics. The effect of keeping these low-level cloud scenes in the CSR product at the seasonal scale is further illustrated in Figure 9. Here, the gain in sampling is computed with all the images (day and night) for the full June-July-August season over the 2 contrasted years of 1984 and 1992 [*Brogniez et al.*, 2004]. For both years, the climatologic maxima of low-level cloudiness off the Angola coast in the southern Atlantic Ocean are shown to be sampled in conditions similar to the adjacent desert areas when the methodology is applied while the pure clear-sky sampling authorized four times less CSR estimations there. Over the ITCZ, the gain is more pronounced over the ocean than over land but in both cases, is smaller than over the subtropics.

3.3. Sensitivity to the Pressure Threshold

[20] Sensitivity analysis of both the contamination of the CSR by misclassified clouds and the gain in sampling is conducted by repeating the above computations for a set of thresholds of 750, 800 and 850 hPa instead of 680 hPa. (Results for 700 hPa are very similar to the 680 hPa and are not shown.) Table 1 shows the dependency of the gain in sampling to the threshold for the contrasted summer seasons of 1984 and 1992. The sensitivity is similar for the two seasons and the percentage of available CSR over the region decreases when the threshold increases, from around 80% for 680 hPa down to around 60% using 850 hPa. The loss of sampling for the lowest threshold is accompanied by a slight decrease of the cloud contamination, which is small in any case. On average over the season and region, the contamination marginally decreases but the improvement reaches 0.1–0.3 K over small parts of the continental ITCZ where the patches of contamination seen in Figure 7 almost disappear.

[21] In summary, the scene selection used for constructing the CSR results in a significant gain in sampling authorizing the building of useful maps down to the daily timescale. The cost of such an enhanced sampling, induced by an imperfect cloud level attribution is small. On the top of being suited for the cloud clearing step, the ISCCP DX other main advantage is its continuous availability over the 1983 onward period allowing the building of the CSR long-term archive which is presented now.

4. Long-Term Clear-Sky Radiance Archive 1983–1997

[22] In the reference paper by *Picon et al.* [2003], the methodology employed to construct a homogenous archive from the original measurements as well as the need for reprocessing the Meteosat WV archive are detailed at length. We here only recall the basics of the technique as well as the differences in implementing it between the present work and this previous effort.

4.1. Building the Homogeneous Long-Term Archive

[23] Two main sources of inhomogeneities characterize the original archive over the July 1983 to February 1997 period. First, four different radiometers were operated with slight differences in the filter functions yielding to inhomogeneous BT series. This can easily be accounted for by converting all the BT into Meteosat-5 equivalent BT, our reference. Second, updates and improvements of the vicar-

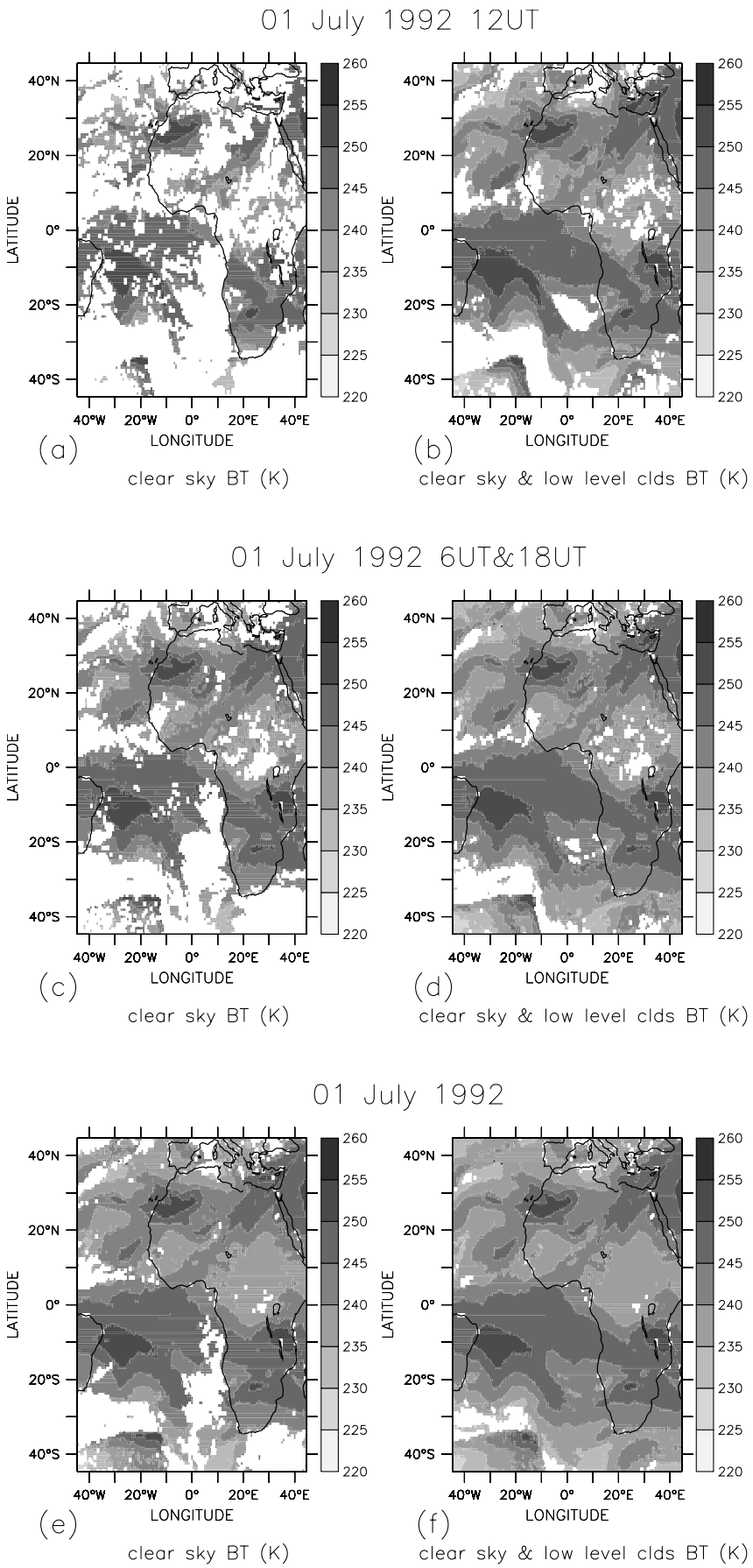
01 July 1992 12UT
01 July 1992 6UT&18UT
01 July 1992
LATITUDE
LONGITUDE
40°N
20°N
0°
20°S
40°S
40°W
20°W
0°
20°E
40°E
260
255
250
245
240
235
230
225
220
(a)
clear sky BT (K)
(b)
clear sky & low level clds BT (K)
(c)
clear sky BT (K)
(d)
clear sky & low level clds BT (K)
(e)
clear sky BT (K)
(f)
clear sky & low level clds BT (K)

Figure 8

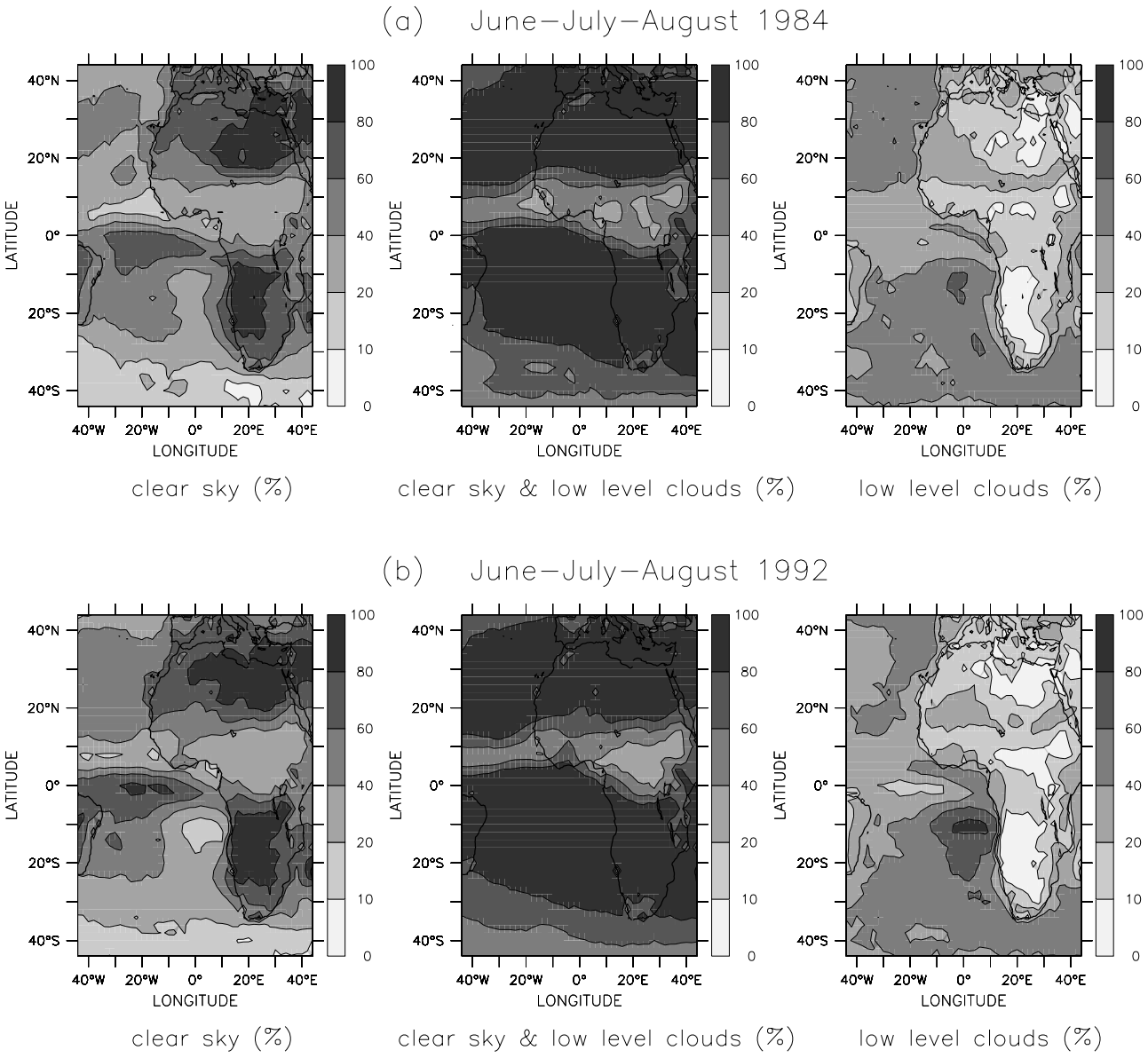

Figure 9. Maps of the percentage of available CSR pixels used to compute the June-July-August seasonal mean for (a) 1984 and (b) 1992 using the pure clear-sky selection (left maps), the low-level cloud ($P_{top} \geq 680$ hPa) + clear-sky selection (middle maps) and the difference, i.e., the low cloud fraction (right maps).

ious calibration technique over the time [*Schmetz and Turpeinen*, 1988; *Schmetz*, 1989; *Van de Berg et al.*, 1995] produce strong step-like changes in the time series of the WV radiances. To account for such changes, P03 developed a root-mean-square normalization technique based on comparisons between the satellite and BT simulated from short time slices of atmospheric analysis around the event to be corrected. Details are provided in the P03 paper. For the CSR archive, the homogenization coefficients are computed using ERA40 (instead of ERA15), the RTTOV-7 radiative code (instead of the code formerly used for the operational calibration [*Schmetz and Turpeinen*, 1988]) and the newly estimated clear-sky scenes using ISCCP-DX data are retained (instead of a threshold-based clear scene selection). The reference period of February 1994, following the latest version of the EUMETSAT nominal calibration, is kept as a reference as in P03. Hence

Figure 8. Maps of pure clear-sky WV BT and clear-sky and low-level clouds ($P_{top} \geq 680$ hPa) WV BT for 1 July 1992. (a and b) The 1200 UT observation is only considered, (c and d) the observations at 0600 UT and 1800 UT only are considered for the daily mean, and (e and f) the eight images provided by the satellite (0000 UT, 0300 UT, 0600 UT, 0900 UT, 1200 UT, 1500 UT, 1800 UT and 2100 UT) are used to compute the daily mean.

Table 1. Percentage of Available CSR for the June-July-August Seasons of 1984 and 1992 According to the Low-Level Cloud Selection Threshold[a]

	JJA 1984	JJA 1992
Clear-sky only	46.7	48.9
Clear-sky + low-level clouds of $P_{top} \geq$		
680 hPa	78.4	79.8
750 hPa	72.5	72.4
800 hPa	65.9	64.7
850 hPa	61.8	59.5

[a]The statistics are computed over the area 45°W–45°E/45°N–45°S.

the CSR archive consists in nominally calibrated and long-term homogenized Meteosat-5 BT.

4.2. Evaluation of the Homogeneity Using Radiosondes

[24] The ECMWF radiosoundings archive contains the operational soundings available for the ERA-40 reanalysis processing [*Uppala et al.*, 2005] and is used to evaluate the stability of the CSR archive over the time. Original profiles of temperature and humidity have been vertically completed to the top of the atmosphere (5.10^{-2} hPa) using climatology, interpolated on fixed pressure levels and extracted over the 45°N–45°S/45°W–45°E region and over the 1983–1996 period. Owing to some issues in the quality of the temperature/humidity measurements and corrections during day (R. Armante, personal communication, 2005), only nighttime soundings are kept in the comparisons. Similarly, soundings reading relative humidity below 5% or in excess of saturation in the free troposphere have been rejected. For each of these profiles, the Meteosat-5 WV channel BT is computed using the RTTOV-7 code. The collocation with the CSR is then made within 0.625°/1h30 precision. Soundings with BT departure from the homogeneous satellite CSR larger than 3 K are also rejected from the comparison. With such stringent quality controls, a limited number of comparisons remain available ranging from 20 up to 80 points per month depending mainly upon seasons (see Figure 10 (top)).

[25] Figure 10 (bottom) shows the difference between the BT simulated from these soundings and the CSR over the archive duration. The mean bias is small (0.3 K) and as expected agrees with the bias of the selected reference period (February 1994) for calibration. The difference between the two sources of information is bounded within −1 K and 1.5 K over the 13 year period. The standard deviation is also small (0.5 K) indicative of similar homogeneity between the in situ archive and the satellite over the period. For information and in completion to P03, Figure 10 (top) shows the comparison to the original archive and recalls, if needed, the importance of the homogenization effort.

4.3. Discussion on the Absolute Calibration

4.3.1. Rationale for an Adjustment

[26] The homogenous database is adjusted on the nominal calibration of Meteosat-5 as of February 1994. Such nominal calibration is performed in a vicarious way using radiosoundings as ancillary data [*Van de Berg et al.*, 1995]. Such an approach has been shown to bias the brightness temperature when compared to other similar instruments flown on board polar and/or geostationary platforms [*Bréon et al.*, 2000; *Sohn et al.*, 2000; *Tjemkes et al.*, 2001]. Operational monitoring of WV radiances at ECMWF has also confirmed a warm artificial bias of 2–3 K for the Meteosat satellite [*Köpken et al.*, 2003]. As a result, a second database is

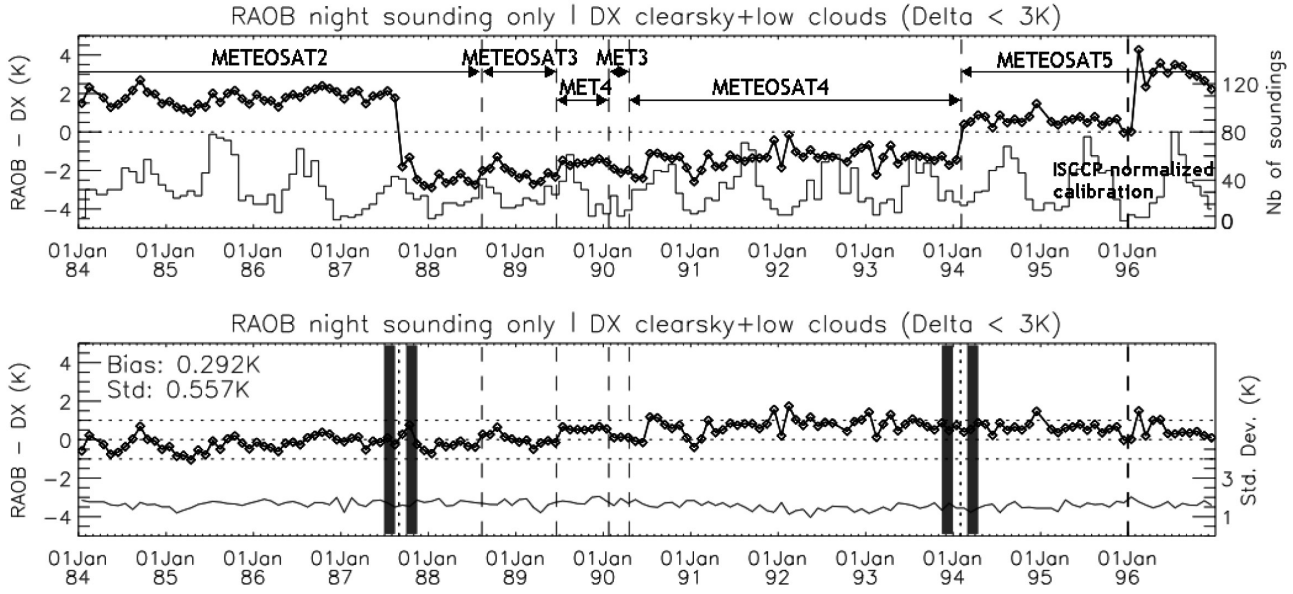

Figure 10. Comparisons between the Meteosat-5 BT simulated from radiosoundings using the RTTOV7 code and the observed BT. Only clear-sky and low-level clouds scenes are considered. (top) Difference before the homogenization step (see text for details) and the number of radiosoundings available within each month and (bottom) difference with the Meteosat-5 homogenized database (diamonds) and the standard deviation of the difference within each month (thin line). Bias and standard deviation (in Kelvins) are indicated. The vertical dashed lines indicate the main radiometric events, and the shaded areas indicate the reference periods [see *Picon et al.*, 2003].

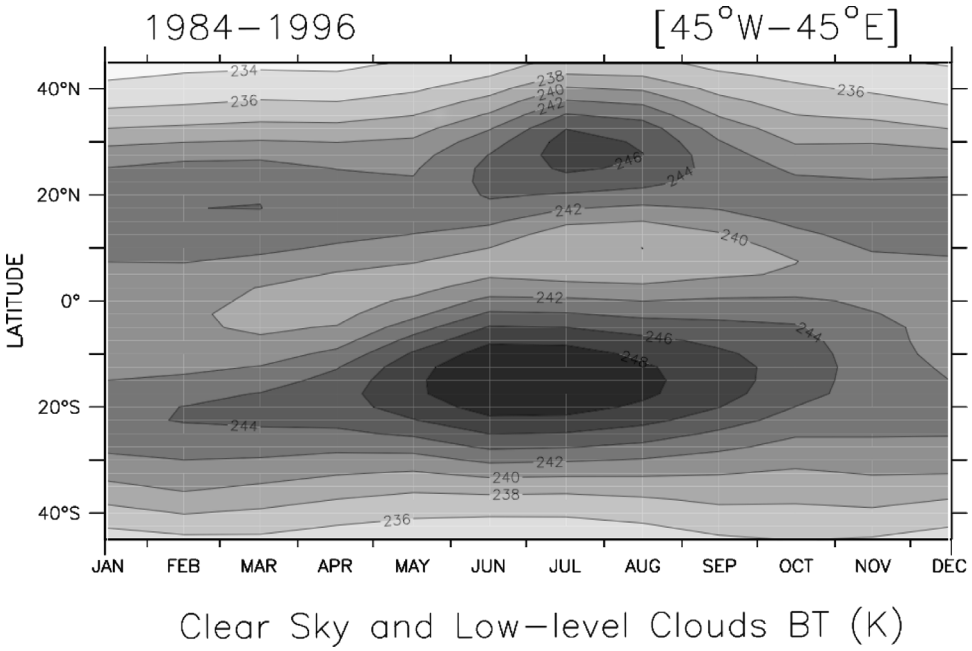

Figure 11. Hovmuller diagram of the mean seasonal cycle of the homogenized Meteosat WV database for the period 1984–1996. The zonal mean is computed over the area 45°W–45°E. The contour interval is 2 K.

constructed to complete the CSR nominally calibrated archive using the NOAA 12 derived intercalibration coefficient data from *Bréon et al.* [2000]. Here, our goal is not to discuss the origin of the calibration bias of the Meteosat WV channel, but is to provide a database consistent with the HIRS 12/NOAA 12 instrument taken as a reference.

4.3.2. Methodology

[27] The methodology used to perform this adjustment of calibration is based on the calibration technique of the Meteosat WV channel [*Van de Berg et al.*, 1995]. The nominal calibration of this channel links the raw digital counts C (unit is cn), obtained from the observational system, to the expected radiance R ($W/m^2/sr$) computed from radio-soundings through

$$R = \alpha(C - C_0) \quad (1)$$

where C_0 is the space count [e.g., *Schmetz*, 1989; *Picon et al.*, 2003] and α the calibration coefficient (in $W/m^2/sr/cn$). *Bréon et al.* [2000] compared the operational Meteosat-5 calibration coefficient and a calibration coefficient derived by collocating the Meteosat count with HIRS 12/NOAA 12 measurements over the 2-year period 1994–1996. The ratio r_α between the HIRS 12 derived and the operational calibration coefficients averages to 0.893 corresponding to a relative bias $\Delta\alpha/\alpha$ of 10.7% in agreement with other evaluations of the operational calibration [*Sohn et al.*, 2000; *Köpken et al.*, 2003]. The main characteristic of this comparison is that r_α exhibits a very low standard deviation of 0.013 (1.5%) over the 2 years period. The maximum departure from the mean values occurs during the spring of 1996 but remains in the order of a few percents in magnitude. Such strong stability allows implementing the correction as a single bias correction of the nominal calibration coefficient all over the archive duration. When compared to the radio-soundings series, the new archive remains similarly stable and exhibits a bias around −3 K in agreement with previous similar comparisons between soundings and polar orbiter based water vapor measurements [e.g., *Soden and Lanzante*, 1996].

4.4. First Analysis

[28] In complement of its very good sampling of the dry subtropical zones, the principal originality of this new Meteosat archive concerns its ability to depict the synoptic-scale variability because of available significant daily maps. As a first illustration, Figure 11 shows the zonal average of the 14 years mean seasonal cycle of the monthly mean of clear-sky brightness temperature. The major signal arises from the large-scale warming (and drying) of the subtropical free troposphere from winter to summer in both hemispheres associated with the seasonal swing of the large-scale tropical circulation. This was already observed with a shorter subset of Meteosat-2 all sky data [*Picon et al.*, 1995] and identified in an ensemble of general circulation models simulations of 20 years as a steady feature of the GCM circulation [*Roca et al.*, 1997] and is here confirmed as a robust climatic feature of the water vapor in the troposphere. Figure 12 shows the zonal average of the multiyear mean of the seasonal cycle of the monthly standard deviation (s) of the clear-sky brightness temperature. This is an index of the short-term variability in the tropospheric water vapor. It indicates that at subtropical latitudes in both hemispheres (20–30°N and 20–30°S), water vapor fluctuates at the synoptic/intraseasonal scale. The differences show that the activity peaks during the boreal winter and spring in the Northern Hemisphere (s $\sim$ 5 K) and decreases during

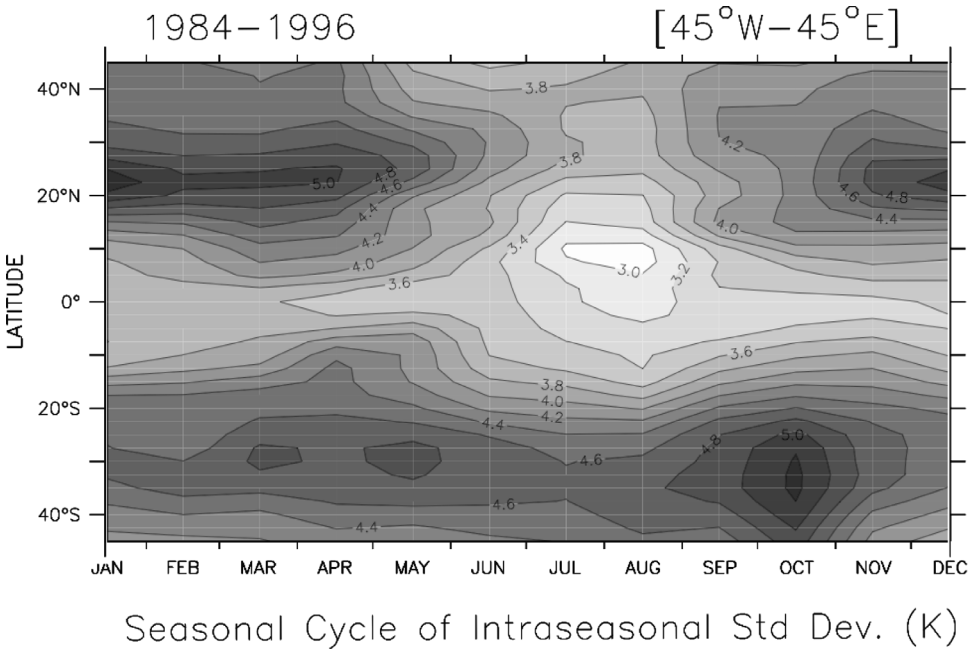

Figure 12. Hovmuller diagram of the mean seasonal cycle of the monthly standard deviation computed from daily maps (in Kelvins) of the Meteosat WV BT for the period 1984–1996. The zonal mean is computed over the area 45°W–45°E. The contour interval is 0.2 K.

summer (s $\sim$ 3 K) while, in the Southern Hemisphere, the standard deviation shows almost no seasonal cycle. This newly documented variability should be further analyzed and related to the water vapor dynamics of the region and will be the topic of future works.

5. Conclusions

[29] A long-term homogeneous archive of Meteosat "water vapor" clear-sky radiance is constructed from the ISCCP-DX data set. Thanks to the simultaneous availability of cloud top information and radiance, a scene selection procedure that keeps low-level cloudiness scenes is implemented. The database (the CSR archive is currently completed up to 2004 (Meteosat-7) following the present approach) covers the July 1983 to February 1997 period with a resolution of 0.625° $\times$ 0.625° over the 45°N–45°S/45°E–45°W region, and a 3 hourly time step. The homogenization is performed as in P03 with some slight changes among which the replacement of ERA15 by ERA40 in the computations. The comparison to the radiosondes archive shows a small standard deviation of the difference of 0.3 K over the period indicative of a fair stability. Absolute calibration issues have emerged in the recent years and are still in the discussions at the space agencies level. A previously proposed alternative to the original approach using radiosondes for calibration based on the NOAA satellite is used to provide a complementary data set. Two databases are hence produced: one with the EUMETSAT nominal absolute calibration and one with the NOAA reference. These new archives will be soon anonymously available on the Institut Pierre Simon Laplace data server "Climserv" at the URL http://climserv.ipsl.polytechnique.fr/les-donnees/clear-sky-wv-radiances.html.

[30] The use of a cloud top pressure based scene selection procedure broadens the usefulness of the WV imagery at the cost of some cloud contamination of the CSR. The constraints on the space/time availability of cloud information isolated the ISCCP-DX data set as the best candidate for such cloud clearing. Consistency with ISCCP cloudiness definition has been pursued in agreement with previous efforts [*Schmetz and Turpeinen*, 1988] and a threshold of 680 hPa is selected. This yields to a significantly enhanced sampling with respect to pure clear sky in the subtropical highs regions over which marginal cloud contamination occurs. On the other hand, over the ITCZ region and more generally where thin cirrus are found to occur, contamination is found to be smaller for a more restrictive threshold selection that also diminishes the gain in sampling. The pressure threshold sensitivity study has indeed revealed that the trade between contamination and the gain in sampling is regionally dependant. A fine tuning of the present approach could employ a seasonally and time varying threshold to get the best sampling at the minimum contamination cost by setting a high threshold over the high cloud areas and a lower threshold over the low cloud deck zones. Similarly the technique could be easily extended to microwave humidity sounders for which the cirrus level misattribution might not be as sensitive as for the IR [e.g., *Greenwald and Christopher*, 2002] but for which a particular effort need to be undertaken for the low-level water clouds.

[31] The present new data set completes the available ones to document the water vapor in the troposphere, and in particular the similar product derived from the NOAA operational meteorological satellite [*Soden and Lanzante*, 1996; *Bates and Jackson*, 2001], and should offer new research opportunities either toward the assimilation for

reanalysis effort [e.g., *Köpken et al.*, 2003] or the climate analysis of the water vapor field. The availability of this new data set also calls for quantitative analysis of the humidity in the troposphere using geophysical parameters derived from CSR [e.g., *Brogniez et al.*, 2005], which is the scope of future works. For instance, preliminary analyses have highlighted a complex mixing of air masses from tropical and extratropical areas that could explain the interannual and intraseasonal variabilities of the FTH over the eastern Mediterranean region [*Brogniez et al.*, 2004].

[32] **Acknowledgments.** Thanks to the ARA team at LMD for sharing with us their version of the radiosondes archive and in particular to R. Armante and C. Stubenrauch for helpful discussions. The help of V. Golea (NASA/GISS) and G. Sèze (LMD) with the DX data set is appreciated. We would like to thank F. M. Bréon (LSCE) for providing us the alternative calibration coefficients and for enriching discussions and J. N. Thépaut (ECMWF) for suggesting the comparison to the soundings archive. We thank also L. Van de Berg (EUMETSAT) for fruitful discussions along the course of the study. The support of K. Ramage and of the IPSL data server "Climserv" is also appreciated. We acknowledge the reviewers for their comments that helped to improve the manuscript.

References

Allan, R., M. Ringer, and A. Slingo (2003), Evaluation of moisture in the Hadley Center climate model using simulations of HIRS water-vapour channel radiances, *Q. J. R. Meteorol. Soc.*, *129*, 3371–3389.

Bates, J., and D. Jackson (2001), Trends in upper-tropospheric humidity, *Geophys. Res. Lett.*, *28*, 1695–1698.

Bony, S., et al. (2006), How well do we understand and evaluate climate change feedback processes?, *J. Clim.*, *19*, 3445–3482.

Bréon, F.-M., D. Jackson, and J. Bates (2000), Calibration of the Meteosat water vapor channel using collocated NOAA/HIRS 12 measurements, *J. Geophys. Res.*, *105*, 11,925–11,933.

Brogniez, H., R. Roca, and L. Picon (2004), Interannual and intraseasonal variabilities of the free tropospheric humidity using Meteosat water vapor channel over the tropics, paper presented at Eumetsat Meteorological Satellite Conference, Prague, Czech Republic, 31–4 June 2004.

Brogniez, H., R. Roca, and L. Picon (2005), Evaluation of the distribution of subtropical free tropospheric humidity in AMIP-2 simulations using Meteosat water vapor channel data, *Geophys. Res. Lett.*, *32*, L19708, doi:10.1029/2005GL024341.

Coakley, J., and F. Bretherton (1982), Cloud cover from high-resolution scanner data: Detecting and allowing for partially filled fields of view, *J. Geophys. Res.*, *87*, 4917–4932.

Diongue, A., J.-P. Lafore, J.-L. Redelsperger, and R. Roca (2002), Numerical study of a Sahelian synoptic weather system: Initiation and mature stages of convection and its interactions with the large-scale dynamics, *Q. J. R. Meteorol. Soc.*, *128*, 1899–1927.

Fischer, H., N. Eigenwillig, and H. Müller (1981), Information content of Meteosat and Nimbus/THIR water vapor channel data: Altitude association of observed phenomena, *J. Appl. Meteorol.*, *20*, 1344–1352.

Greenwald, T. J., and S. A. Christopher (2002), Effect of cold clouds on satellite measurements near 183 GHz, *J. Geophys. Res.*, *107*(D13), 4170, doi:10.1029/2000JD000258.

Held, I., and B. Soden (2000), Water vapor feedback and global warming, *Annu. Rev. Energy Environ.*, *25*, 441–475.

Jin, Y., and W. Rossow (1997), Detection of cirrus overlapping low level clouds, *J. Geophys. Res.*, *102*, 1727–1737.

Joseph, B., and M. Moustaoui (2000), Transport, moisture, and rain in a simple monsoonlike flow, *J. Atmos. Sci.*, *57*, 1817–1838.

Köpken, C., J.-N. Thépaut, and G. Kelly (2003), Assimilation of geostationary WV radiances from GOES and Meteosat at ECMWF, *Res. Rep. 14*, Eumetsat/ECMWF Fellowship Program, Reading, U. K.

Lanzante, J., and G. Gahrs (2000), The "clear-sky bias" of TOVS upper-tropospheric humidity, *J. Clim.*, *13*, 4034–4040.

Marenco, A., et al. (1998), Measurement of ozone and water vapor by Airbus in-service aircraft: The MOZAIC airborne program, An overview, *J. Geophys. Res.*, *103*, 25,631–25,642.

Mathieu, A., G. Sèze, A. Lahellec, C. Guerin, and A. Weill (2003), Characterization of the cloud-topped boundary layer at the synoptic scale using AVHRR observations during the SEMAPHORE experiment, *J. Appl. Meteorol.*, *42*, 1720–1730.

Matricardi, M., F. Chevallier, G. Kelly, and J.-N. Thépaut (2004), An improved general fast radiative transfer model for the assimilation of radiance observations, *Q. J. R. Meteorol. Soc.*, *130*, 153–173.

McClatchey, R., R. Fenn, J. Selby, F. Volz, and J. Garing (1971), Optical properties of the atmosphere, *Air Force Cambridge Rep. AFCRL-71–0279*, 85 pp., Hanscom Field, Mass.

McMillin, L., and C. Dean (1982), Evaluation of a new operational technique for producing clear radiance, *J. Appl. Meteorol.*, *21*, 1005–1014.

Minnis, P., P. W. Heck, D. F. Young, C. W. Fairall, and J. B. Snider (1992), Stratocumulus cloud properties derived from simultaneous satellite and island-based instrumentation during FIRE, *J. Appl. Meteorol.*, *31*, 317–339.

Morel, P., M. Desbois, and G. Szejwach (1978), A new insight into the troposphere with the water vapor channel of Meteosat, *Bull. Am. Meteorol. Soc.*, *102*, 373–394.

Picon, L., and M. Desbois (1990), Relation between Meteosat water vapor radiance fields and large scale tropical circulation features, *J. Clim.*, *3*, 865–876.

Picon, L., S. Fongang, G. Seze, and M. Desbois (1995), African and Atlantic short-term climatic variations described from Meteosat water vapor channel, *Ann. Geophys.*, *13*, 768–781.

Picon, L., R. Roca, S. Serrar, J. L. Monge, and M. Desbois (2003), A new Meteosat "water vapor" archive for climate studies, *J. Geophys. Res.*, *108*(D10), 4301, doi:10.1029/2002JD002640.

Pierrehumbert, R. T. (1995), Thermostats, radiator fins and the local runaway greenhouse, *J. Atmos. Sci.*, *52*, 1784–1806.

Pierrehumbert, R. T., and R. Roca (1998), Evidence for control of Atlantic subtropical humidity by large scale advection, *Geophys. Res. Lett.*, *24*, 4537–4540.

Ramond, D., H. Corbin, M. Desbois, G. Szejwach, and P. Waldteufel (1981), The dynamics of polar jet streams as depicted by the Meteosat WV channel radiance field, *Mon. Weather Rev.*, *109*, 2164–2176.

Ringer, M., J. Edwards, and A. Slingo (2003), Simulation of satellite channel radiances in the Met Office Unified Model, *Q. J. R. Meteorol. Soc.*, *129*, 1169–1190.

Roca, R., L. Picon, M. Desbois, H. Le Treut, and J.-J. Morcrette (1997), Direct comparison between Meteosat water vapor channel and GCM results, *Geophys. Res. Lett.*, *24*, 147–150.

Rossow, W., and L. Garder (1993), Cloud detection using satellite measurements of infrared and visible radiances for ISCCP, *J. Clim.*, *6*, 2341–2369.

Rossow, W., and R. Schiffer (1991), ISCCP cloud data products, *Bull. Am. Meteorol. Soc.*, *72*, 2–20.

Rossow, W., and R. Schiffer (1999), Advances in understanding clouds from ISCCP, *Bull. Am. Meteorol. Soc.*, *80*, 2269–2287.

Rossow, W., L. Garder, P. Lu, and A. Walker (1991), International satellite cloud climatology project (ISCCP): Documentation of cloud data, *WMO/TD 266*, World Meteorol. Org., Geneva, Switzerland.

Schmetz, J. (1989), Operational calibration of the Meteosat water vapor channel by calculated radiances, *Appl. Opt.*, *28*, 3030–3038.

Schmetz, J., and O. Turpeinen (1988), Estimation of the upper tropospheric relative humidity field from Meteosat water vapor image data, *J. Appl. Meteorol.*, *27*, 889–899.

Smith, E., and L. Shi (1992), Surface forcing of the infrared cooling profile over the Tibetan plateau. Part 1: Influence of relative longwave radiative heating at high altitude, *J. Atmos. Sci.*, *49*, 805–822.

Soden, B., and F. Bretherton (1993), Upper tropospheric relative humidity from the GOES 6.7 μm channel: Method and climatology for July 1987, *J. Geophys. Res.*, *98*, 16,669–16,688.

Soden, B., and F. Bretherton (1994), Evaluation of water vapor distribution in general circulation models using satellite observations, *J. Geophys. Res.*, *99*, 1187–1210.

Soden, B., and J. Lanzante (1996), An assessment of satellite and radiosondes climatologies of upper-tropospheric water vapor, *J. Clim.*, *9*, 1235–1250.

Sohn, B.-J., J. Schmetz, S. Tjemkes, M. Koenig, H. Lutz, A. Arriaga, and E. Chung (2000), Intercalibration of the Meteosat-7 water vapor channel with SSM/T-2, *J. Geophys. Res.*, *105*, 15,673–15,680.

Spencer, R., and W. Braswell (1997), How dry is the tropical free troposphere? Implications for a global warming theory, *Bull. Am. Meteorol. Soc.*, *78*, 1097–1106.

Stubenrauch, C., W. Rossow, F. Chéruy, A. Chédin, and N. Scott (1999), Clouds as seen by satellite sounders (3I) and imagers (ISCCP). Part 1: Evaluation of cloud parameters, *J. Clim.*, *12*, 2189–2213.

Tjemkes, S., M. Koenig, M. Lutz, L. Van de Berg, and J. Schmetz (2001), Calibration of Meteosat water vapor channel observations with independent satellite observations, *J. Geophys. Res.*, *106*, 5199–5209.

Udelhofen, P., and D. Hartmann (1995), Influence of a tropical cloud system on the relative humidity in the upper troposphere, *J. Geophys. Res.*, *100*, 7423–7440.

Uppala, S. M., et al. (2005), The ERA-40 re-analysis, *Q. J. R. Meteorol. Soc.*, *131*, 2961–3012.

Van de Berg, L., J. Schmetz, and J. Whitlock (1995), On the calibration of the Meteosat water vapor channel, *J. Geophys. Res.*, *100*, 21,069–21,076.

Waugh, D. W. (2005), Impact of potential vorticity intrusions on subtropical upper tropospheric humidity, *J. Geophys. Res.*, *110*, D11305, doi:10.1029/2004JD005664.

Wu, X., J. Bates, and S. Singh Kahlsa (1993), A climatology of the water vapor band brightness temperature from NOAA operational satellites, *J. Clim.*, *6*, 1282–1300.

Yang, H., and R. T. Pierrehumbert (1994), Production of dry air by isentropic mixing, *J. Atmos. Sci.*, *51*, 3437–3454.

H. Brogniez, Centre d'Etude des Environnements Terrestre et Planétaires, Centre National de la Recherche Scientifique, Institut Pierre-Simon Laplace, F-78140 Velizy, France. (helene.brogniez@cetp.ipsl.fr)

L. Picon and R. Roca, Laboratoire de Météorologie Dynamique, Centre National de la Recherche Scientifique/Institut Pierre-Simon Laplace, F-75252 Paris, France.